A Lower Bound for the Error Covariance of Radio SLAM with Terrestrial Signals of Opportunity

Alexander A. Nguyen, Zeinab Shadram, and Zaher M. Kassas
University of California, Irvine

BIOGRAPHIES

Alexander A. Nguyen is a Ph.D. student in the Department of Mechanical and Aerospace Engineering at the University of California, Irvine and a member of the Autonomous Systems Perception, Intelligence, and Navigation (ASPIN) Laboratory. He received a B.S. in Mechanical Engineering with Honors from the University of California, Santa Barbara. His current research interests include collaborative opportunistic navigation, estimation theory, and motion planning.

Zeinab Shadram is a postdoctoral scholar at the University of California, Irvine and member of the Autonomous Systems Perception, Intelligence, and Navigation (ASPIN) Laboratory. She received a B.S. and a M.S. in Aerospace Engineering from Sharif University of Technology (SUT) in Tehran, and a Ph.D. in Mechanical and Aerospace Engineering from the University of California, Irvine (UCI). Her research interests include opportunistic navigation, wireless communication systems, and software-defined radio.

Zaher (Zak) M. Kassas is an associate professor at the University of California, Irvine and director of the Autonomous Systems Perception, Intelligence, and Navigation (ASPIN) Laboratory. He is also director of the U.S. Department of Transportation Center: CARMEN (Center for Automated Vehicle Research with Multimodal AssurEd Navigation), focusing on navigation resiliency and security of highly automated transportation systems. He received a B.E. in Electrical Engineering from the Lebanese American University, an M.S. in Electrical and Computer Engineering from The Ohio State University, and an M.S.E. in Aerospace Engineering and a Ph.D. in Electrical and Computer Engineering from The University of Texas at Austin. He is a recipient of the 2018 National Science Foundation (NSF) Faculty Early Career Development Program (CAREER) award, 2019 Office of Naval Research (ONR) Young Investigator Program (YIP) award, 2018 IEEE Walter Fried Award, 2018 Institute of Navigation (ION) Samuel Burka Award, and 2019 ION Col. Thomas Thurlow Award. His research interests include cyber-physical systems, estimation theory, navigation systems, autonomous vehicles, and intelligent transportation systems.

ABSTRACT

A lower bound for the error covariance of radio simultaneous localization and mapping (SLAM) with terrestrial signals of opportunity (SOPs) is derived. The following problem is considered. An unmanned aerial vehicle (UAV) equipped with an on-board receiver extracts psuedorange measurements from SOP towers with unknown emitter positions and SOP towers with known emitter positions. Each SOP tower contains dynamic, stochastic clock error states (bias and drift). An extended Kalman filter (EKF) is employed to fuse the psuedorange measurements to simultaneously localize the UAV and SOP towers, together with estimating the difference between the receiver's and each SOP's clock bias and clock drift terms. It is shown that the so-called radio SLAM base case is observable, in which a UAV with imperfect knowledge about its initial states is navigating in an environment containing one *unknown* SOP tower and two *partially known* SOP towers (i.e., towers whose position are known, but clock bias and drift states are unknown). A lower bound on the EKF estimation error covariance matrix is derived and demonstrated numerically. Monte Carlo simulation results are presented demonstrating the derived lower bound for a UAV navigating in a radio SLAM fashion without global navigation satellite systems (GNSS) signals. Experimental results are presented for a UAV with an initial estimate of its position making pseudorange measurements to two partially known and one unknown cellular SOP. The UAV achieves a two-dimensional (2-D) position root-mean squared error (RMSE) of 10.76 m over a trajectory of 600 m.

Preprint of the 2021 ION GNSS+ Conference St. Louis, MO, September 20–24, 2021

I. INTRODUCTION

Autonomous vehicles typically depend on global navigation satellite systems (GNSS) for their on-board navigation system. Alarmingly, this reliance is not sufficient to provide resilient and precise vehicle positioning all the time. Specifically, there are GNSS-challenged environments such as deep urban canyons [1], indoors [2], and those under malicious attacks (e.g., spoofing [3] or jamming [4]), which require an alternative to GNSS for safe and reliable navigation. These alternative approaches include the use of sensors with complementary sensing modalities (e.g., lasers [5], ultrasonics [6], cameras [7], and inertial measurement units [8]). Another approach is radionavigation-based, which utilizes ambient signals of opportunity (SOPs) in the environment [9], such as AM/FM radio [10, 11], cellular [12–15], digital television [16, 17], low Earth orbit (LEO) satellites [18–21], and WiFi [22, 23]. These signals were not intended for position, navigation, and timing (PNT) purposes; nevertheless, the literature has shown that they can be exploited for such purposes. SOPs are abundant, are transmitted in a wide range of frequencies, are more powerful than GNSS signals, and are geometrically diverse. These attributes address the inherent limitations of GNSS signals. However, unlike the states of a GNSS space vehicle, SOP states are typically unknown during navigation which requires them to be estimated on the fly. This is similar to the simultaneous localization and navigation (SLAM) estimation problem in robotics [24, 25]. In traditional SLAM, an agent constructs a map of the environment while simultaneously localizing itself within this map. Typically, an environment is composed of static landmarks, e.g., walls, posts, and corners. However, unlike traditional SLAM, SOPs are mapped as spatio-temporal landmarks composed of dynamic, stochastic states (i.e., clock error terms). The problem of simultaneously mapping ambient SOPs while localizing a vehicle-mounted receiver using PNT information is referred to as radio SLAM [26, 27].

Past literature in radionavigation considered fundamental questions pertaining to deterministic nonlinear observability of collaborative opportunistic navigation [28], stochastic observability of radio SLAM [29], radio SLAM filter boundedness [30], radio SLAM performance [31], motion planning in radio SLAM environments [32], and communication and information fusion strategies for collaborative radio SLAM [33, 34]. Nevertheless, lower bounds for the radio SLAM problem have not been established yet. These bounds are of considerable importance as they establish the bounds on the achievable performance in an unknown or a partially known SOP environment. This paper is a first attempt at addressing this. Previous work has derived expressions for calculating uniform bounds of the estimation error covariance by ensuring uniform controllability and uniform observability are satisfied simultaneously [35]. Furthermore, other work established performance bounds for the traditional SLAM problem [36–41]. However, these bounds do not apply to the problem considered in this paper, since radio SLAM utilizes a different measurement model and the state space contains dynamic, stochastic landmark states.

This paper derives a lower bound for the estimation error covariance of an extended Kalman filter (EKF)-based radio SLAM framework. The following problem is considered. An unmanned aerial vehicle (UAV) equipped with an on-board receiver extracts psuedorange measurements from SOP towers with unknown emitter positions and SOP towers with known emitter positions. Each SOP tower contains dynamic, stochastic clock error states which are estimated as the difference between the receiver's and each SOP's clock bias and clock drift terms. This EKF fuses these measurements together for simultaneous receiver and SOP tower localization and clock error estimation.

The remainder of this paper is organized as follows. Section II describes the receiver and SOP dynamics models, modified clock error states, and the EKF model. Section III contains a brief observability analysis pertaining to the radio SLAM base case (i.e., UAV with imperfect knowledge of its initial states using signals from two partially known cellular SOPs and an unknown cellular SOP). Section IV derives a lower bound for the radio SLAM problem as a function of time and number of partially known and unknown SOPs, which is subsequently demonstrated with simulation results. Section V presents experimental results conducted on a UAV performing radio SLAM without GNSS signals. Section IV contains concluding remarks.

II. MODEL DESCRIPTION

This section presents the dynamics model for a UAV-mounted receiver and a terrestrial SOP tower, the modified clock error states, and the EKF model. Only the UAV's two-dimensional (2-D) position is considered, as an altimeter or barometric pressure sensor can be used to estimate the UAV's altitude.

A. Receiver Dynamics Model

The UAV-mounted receiver states consist of the 2-D positions $\boldsymbol{r}_r = [x_r,\ y_r]^{\mathsf{T}}$, 2-D velocities $\dot{\boldsymbol{r}}_r = [\dot{x}_r,\ \dot{y}_r]^{\mathsf{T}}$, and clock error states $\boldsymbol{x}_{\text{clk},r} = [c\delta t_r,\ c\dot{\delta t}_r]^{\mathsf{T}}$ where $\delta t_r(k)$ and $\dot{\delta t}_r(k)$ are the receiver's clock bias and drift, respectively, and c is the speed of light. The receiver's position and velocity states are assumed to adhere to a velocity random walk model [42]. Therefore, the UAV-mounted receiver can be modeled as the following discrete-time model

$$\boldsymbol{x}_{\text{r}}\left(k+1\right) = \mathbf{F}_r\, \boldsymbol{x}_{\text{r}}(k) + \boldsymbol{w}_r(k), \quad k = 0, 1, 2, ...,$$

where

$$\boldsymbol{x}_{\text{r}} = [\boldsymbol{r}_r^{\mathsf{T}},\ \dot{\boldsymbol{r}}_r^{\mathsf{T}},\ \boldsymbol{x}_{\text{clk},r}^{\mathsf{T}}]^{\mathsf{T}},$$
$$\mathbf{F}_r = \begin{bmatrix} \mathbf{I}_{2\times 2} & T\mathbf{I}_{2\times 2} & \mathbf{0}_{2\times 2} \\ \mathbf{0}_{2\times 2} & \mathbf{I}_{2\times 2} & \mathbf{0}_{2\times 2} \\ \mathbf{0}_{2\times 2} & \mathbf{0}_{2\times 2} & \mathbf{F}_{\text{clk}} \end{bmatrix}, \quad \mathbf{F}_{\text{clk}} = \begin{bmatrix} 1 & T \\ 0 & 1 \end{bmatrix},$$

where $\boldsymbol{w}_{\text{r}}$ is the receiver's process noise, which is modeled as a discrete-time zero-mean white noise sequence with covariance $\mathbf{Q}_r = \text{diag}[\mathbf{Q}_{\text{pv}}, \mathbf{Q}_{\text{clk},r}]$, with

$$\mathbf{Q}_{\text{pv}} = \begin{bmatrix} \tilde{q}_x\frac{T^3}{3} & 0 & \tilde{q}_x\frac{T^2}{2} & 0 \\ 0 & \tilde{q}_y\frac{T^3}{3} & 0 & \tilde{q}_y\frac{T^2}{2} \\ \tilde{q}_x\frac{T^2}{2} & 0 & \tilde{q}_x T & 0 \\ 0 & \tilde{q}_y\frac{T^2}{2} & 0 & \tilde{q}_y T \end{bmatrix}, \quad \mathbf{Q}_{\text{clk},r} = c^2 \begin{bmatrix} S_{\tilde{w}_{\delta t_r}} T + S_{\tilde{w}_{\delta i_r}}\frac{T^3}{3} & S_{\tilde{w}_{\delta i_r}}\frac{T^2}{2} \\ S_{\tilde{w}_{\delta i_r}}\frac{T^2}{2} & S_{\tilde{w}_{\delta i_r}} T \end{bmatrix},$$

where T is the sampling time and $\tilde{q}_x$ and $\tilde{q}_y$ are the continuous-time x and y acceleration noise power spectral densities. The terms $S_{\tilde{w}_{\delta t_r}}$ and $S_{\tilde{w}_{\delta i_r}}$ are the clock bias and drift process noise power spectra, which can be related to the power-law coefficients, $\left\{h_{\alpha,s_i}\right\}_{\alpha=-2}^{2}$; laboratory experiments have shown that the power spectral density of the fractional frequency deviation of an oscillator from nominal frequency to be appropriately approximated by $S_{\tilde{w}_{\delta t_r}} \approx \frac{h_{0,r}}{2}$ and $S_{\tilde{w}_{\delta i_r}} \approx 2\pi^2 h_{-2,r}$ [43].

B. SOP Dynamics Model

Each SOP is assumed to emanate from a spatially-stationary terrestrial transmitter. The states will consist of 2-D positions $\boldsymbol{r}_{s_i} = [x_{s_i},\ y_{s_i}]^{\mathsf{T}}$ and clock error states $\boldsymbol{x}_{\text{clk},s_i} = [c\delta t_{s_i},\ c\dot{\delta t}_{s_i}]^{\mathsf{T}}$, where $\delta t_{s_i}(k)$ and $\dot{\delta t}_{s_i}(k)$ are the i^{th} SOP's clock bias and drift, respectively, with $i = 1, \ldots, M$, where $M \triangleq n + m$ is the total number of SOPs in the environment with n being the number of partially known SOPs and m being the number of unknown SOPs. The i^{th} terrestrial SOP's discretized state-space model can be described by

$$\boldsymbol{x}_{s_i}\left(k+1\right) = \mathbf{F}_s\, \boldsymbol{x}_{s_i}(k) + \boldsymbol{w}_{s_i}(k), \quad k = 0, 1, 2, ...,$$

where

$$\boldsymbol{x}_{s_i} = [\boldsymbol{r}_{s_i}^{\mathsf{T}},\ \boldsymbol{x}_{\text{clk,s}_i}^{\mathsf{T}}]^{\mathsf{T}}$$
$$\mathbf{F}_s = \text{diag}[\mathbf{I}_{2\times 2}, \mathbf{F}_{\text{clk}}]$$

where $\boldsymbol{w}_{s_i}$ is the i^{th} terrestrial SOP's process noise, modeled as a discrete-time zero-mean white noise sequence with covariance $\mathbf{Q}_{s_i} = \text{diag}[\mathbf{0}_{2\times 2}, \mathbf{Q}_{\text{clk},s_i}]$. The $\mathbf{Q}_{\text{clk},s_i}$ covariance matrix is identical to $\mathbf{Q}_{\text{clk},r}$, except that $S_{\tilde{w}_{\delta t_r}}$ and $S_{\tilde{w}_{\dot{\delta t}_r}}$ are replaced with SOP-specific spectra $S_{\tilde{w}_{\delta t,s,i}}$ and $S_{\tilde{w}_{\dot{\delta t},s,i}}$. These spectra terms are modeled similarly to the receiver spectra but with SOP-specific values h_{0,s_i} and h_{-2,s_i}.

C. Modified Clock Error States

Estimating the individual clock error terms for the receiver and each respective SOP could yield a stochastically unobservable system with diverging estimation error variances [29]. Thus, the modified clock bias and clock drift states are redefined to be the difference between the receiver's and SOPs' clock error terms, according to

$$c\delta t_i \triangleq c\delta t_r - c\delta t_{s_i}, \quad i = 1, \ldots, M.$$
$$c\dot{\delta t}_i \triangleq c\dot{\delta t}_r - c\dot{\delta t}_{s_i}$$

Now, the clock states are given as $\boldsymbol{x}_{\text{clk},i} \triangleq \left[c\delta t_i,\ c\dot{\delta} t_i\right]^{\mathsf{T}}$, where the SOP state vector is redefined as $\boldsymbol{x}_{s_i} = \left[\boldsymbol{r}_{s_i},\ \boldsymbol{x}_{\text{clk},i}\right]^{\mathsf{T}}$. The new clock dynamics are given by

$$\boldsymbol{x}_{\text{clk},i}(k+1) = \mathbf{F}_{\text{clk}}\boldsymbol{x}_{\text{clk},i}(k) + \boldsymbol{w}_{\text{clk},i}(k), \quad k = 0, 1, 2, \ldots,$$

where $\boldsymbol{w}_{\text{clk},i}$ is the modified clock error state's process noise, which is modeled as a discrete-time zero-mean white noise sequence with covariance $\mathbf{Q}_{\text{clk},i} = \mathbf{Q}_{\text{clk},r} + \mathbf{Q}_{\text{clk},s_i}$.

D. EKF Model

The EKF estimates the UAV-mounted receiver's position and velocity, n SOP tower's modified clock error states, and m SOP tower's position and modified clock error states, namely

$$\boldsymbol{x} \triangleq [\boldsymbol{r}_r^{\mathsf{T}},\ \dot{\boldsymbol{r}}_r^{\mathsf{T}},\ \boldsymbol{x}_{\text{clk},1}^{\mathsf{T}}, \ldots, \boldsymbol{x}_{\text{clk},n}^{\mathsf{T}},\ \boldsymbol{x}_{s_{n+1}}^{\mathsf{T}}, \ldots,\ \boldsymbol{x}_{s_M}^{\mathsf{T}}]^{\mathsf{T}}.$$

Note that $\boldsymbol{x}$ may be expressed as $\boldsymbol{x} = \mathbf{T}\boldsymbol{x}'$, where $\boldsymbol{x}'$ is the non-modified EKF state vector and $\mathbf{T}$ is some permutation matrix which can be readily calculated for state transformation. The pseudorange measurements made by the receiver on the i^{th} SOP tower is related to the receiver's and SOPs' states by

$$z_{s_i}(k) = \underbrace{\left\|\boldsymbol{r}_r(k) - \boldsymbol{r}_{s_i}\right\|_2 + c\delta t_i(k)}_{h_i[\boldsymbol{x}(k)]} + v_{s_i}(k), \quad i = 1, \ldots, M, \tag{1}$$

where $\|\cdot\|_2$ is the Euclidean norm and v_{s_i} is the measurement noise, which is modeled as a zero-mean white Gaussian sequence with variance $\sigma_{s,i}^2$. It is assumed that the measurement noise is uncorrelated across the different SOPs.

III. BASE CASE OBSERVABILITY ANALYSIS

This section shows that the radio SLAM base case, defined as a UAV with imperfect knowledge of its initial states in an environment with $n = 2$ partially known (mapped) and $m = 1$ unknown SOP towers, to be observable. Moreover, this analysis shows the minimum number of SOP towers needed to guarantee an observable system in an arbitrary environment. This is achieved by studying the rank of the l-step observability matrix. The following assumptions are necessary to ensure the l-step observability matrix does not lose rank due to receiver trajectory or singular geometry.

- A1. The terrestrial SOPs are not colocated
- A2. The receiver is not stationary and does not move along a trajectory collinear to any terrestrial SOP line-of-sight vectors.
- A3. The receiver's distance to each SOP is bounded at all time, i.e., $d_{\min} < \|\boldsymbol{r}_r(k) - \boldsymbol{r}_{s_i}\|_2 < d_{\max},\ \forall\ k > 0$, and $\forall\ i = 1, \cdots, M$, where $d_{\min}$ is the minimum distance to the SOP (to ensure the UAV does not "exactly" fly over the SOP) and $d_{\max}$ is the maximum distance to the SOP (to ensure the UAV does not fly very far from the SOPs, making their geometry in the "far-field," which appears as if they are collocated).

A. Theoretical Background: Observability of Linear and Nonlinear Systems

Consider the discrete-time linear time-varying (LTV) system

$$\begin{aligned} \boldsymbol{x}(k+1) &= \mathbf{F}(k)\boldsymbol{x}(k) + \mathbf{\Gamma}(\mathbf{k})\boldsymbol{u}(k) \\ \boldsymbol{y}(k) &= \mathbf{H}(k)\boldsymbol{x}(k) \end{aligned} \tag{2}$$

where $\boldsymbol{x} \in \mathbb{R}^{\text{n}_\text{x}}$ is the system's state vector, $\boldsymbol{u} \in \mathbb{R}^{\text{n}_\text{u}}$ is the system's input vector, and $\boldsymbol{y} \in \mathbb{R}^{\text{n}_\text{y}}$ is the system's measurement vector. The observability of a LTV system is typically determined by studying the rank of the observability Grammian or the observability matrix. The following theorem states a necessary and sufficient condition for LTV observability through the l-step observability matrix [44]. THEOREM III.1: The discrete-time LTV system is l-step observable if and only if the l-step observability matrix, defined as

$$\boldsymbol{\mathcal{O}}(k, k+l) \triangleq \begin{bmatrix} \mathbf{H}(k) \\ \mathbf{H}(k+1)\mathbf{\Phi}(k+1,k) \\ \mathbf{H}(k+2)\mathbf{\Phi}(k+2,k) \\ \vdots \\ \mathbf{H}(k+l-1)\mathbf{\Phi}(k+l-1,k) \end{bmatrix} \tag{3}$$

is full rank, i.e., $\text{rank}\big[\boldsymbol{\mathcal{O}}(k, k+l)\big] = \text{n}_\text{x}$. The matrix function $\boldsymbol{\Phi}(k, j)$ is the discrete-time transition matrix, which is defined as

$$\boldsymbol{\Phi}(k,j) \triangleq \begin{cases} \mathbf{F}(k-1)\mathbf{F}(k-2)\cdots\mathbf{F}(j), & k \geq j+1 \\ \mathbf{I}, & k = j \end{cases}$$

This observability analysis can be extended to nonlinear systems by linearizing the state transition and observation models to obtain $\mathbf{F}(\text{k})$, $\boldsymbol{\Gamma}(\text{k})$, and $\mathbf{H}(\text{k})$, which establishes observability results only valid locally. More generally, a nonlinear system may be characterized as observable, locally observable, weakly observable, or locally weakly observable [45].

B. Observability Analysis

This analysis looks to classify observability for a discrete-time LTV system by studying the rank of the l-step observability matrix. The state vector and dynamics matrix for the base case is defined as

$$\boldsymbol{x} \triangleq [\boldsymbol{r}_r^\mathsf{T},\ \dot{\boldsymbol{r}}_r^\mathsf{T},\ \boldsymbol{x}_{\text{clk},1}^\mathsf{T},\ \boldsymbol{x}_{\text{clk},2}^\mathsf{T},\ \boldsymbol{x}_{s_3}^\mathsf{T}]^\mathsf{T}, \tag{4}$$

$$\mathbf{F} = \begin{bmatrix} \mathbf{I}_{2\times2} & T\mathbf{I}_{2\times2} & \mathbf{0}_{2\times2} & \mathbf{0}_{2\times2} & \mathbf{0}_{2\times4} \\ \mathbf{0}_{2\times2} & \mathbf{I}_{2\times2} & \mathbf{0}_{2\times2} & \mathbf{0}_{2\times2} & \mathbf{0}_{2\times4} \\ \mathbf{0}_{2\times2} & \mathbf{0}_{2\times2} & \mathbf{F}_\text{clk} & \mathbf{0}_{2\times2} & \mathbf{0}_{2\times4} \\ \mathbf{0}_{2\times2} & \mathbf{0}_{2\times2} & \mathbf{0}_{2\times2} & \mathbf{F}_\text{clk} & \mathbf{0}_{2\times4} \\ \mathbf{0}_{4\times2} & \mathbf{0}_{4\times2} & \mathbf{0}_{4\times2} & \mathbf{0}_{4\times2} & \mathbf{F}_{s_3} \end{bmatrix}. \tag{5}$$

The linearized measurement model yields the following observation Jacobian matrix

$$\begin{aligned} \boldsymbol{\xi}_i(k) &\triangleq \frac{\boldsymbol{r}_r(k) - \boldsymbol{r}_{s_i}}{\|\boldsymbol{r}_r(k) - \boldsymbol{r}_{s_i}\|_2}, \quad \forall i = 1,2,3 \\ \mathbf{H}_{r_i}(k) &= [\boldsymbol{\xi}_i^\mathsf{T}(k),\ \mathbf{0}_{1\times2}],\ \mathbf{H}_{s_i}(k) = [-\boldsymbol{\xi}_i^\mathsf{T}(k),\ \boldsymbol{h}_\text{clk}]^\mathsf{T},\ \boldsymbol{h}_\text{clk} = [1,\ 0], \\ \mathbf{H}(k) &= \begin{bmatrix} \mathbf{H}_{r_1}(k) & \boldsymbol{h}_\text{clk} & \mathbf{0}_{1\times2} & \mathbf{0}_{1\times4} \\ \mathbf{H}_{r_2}(k) & \mathbf{0}_{1\times2} & \boldsymbol{h}_\text{clk} & \mathbf{0}_{1\times4} \\ \mathbf{H}_{r_3}(k) & \mathbf{0}_{1\times2} & \mathbf{0}_{1\times2} & \mathbf{H}_{s_3}(k) \end{bmatrix}. \end{aligned} \tag{6}$$

The l-step observability matrix $\boldsymbol{\mathcal{O}}(k, k+l)$ is of dimension $l \cdot (n+m) \times 4 + 2n + 4m$. One necessary condition for the observability matrix to be full rank is that $l \cdot (n+m) \geq 4 + 2n + 4m$, i.e., the UAV makes measurements at l epochs to the M terrestrial SOP towers. Symbolic computations done in software found the l-step observability matrix to achieve full rank when $l \geq 4$ for the radio SLAM base case. Further generalized, a given system will always be l-step observable with $n \geq 2$ and $m \geq 1$ for $l \geq 4$. Note, this result is the same as the l-step criteria found in the observability analysis for a UAV performing opportunistic navigation [30]. The results of this study are valid only locally and deterministically, i.e., no process or measurement noise and no initial uncertainty. However, these result can be extended to stochastic systems by introducing noise to the position unit vectors $\boldsymbol{\xi}_i'(k) = \boldsymbol{\xi}_i(k) + \boldsymbol{w}_{\xi_i}(k)$. By invoking the stated assumptions A1 - A3, the addition of process noise will not change the structure nor the rank of $\mathbf{H}(k)$. Thus, the deterministic observability analysis still holds for a system with noise [46].

IV. RADIO SLAM PERFORMANCE ANALYSIS

This section derives a lower bound for the radio SLAM performance as a function of time and partially known and unknown SOP towers in the environment. The m unknown SOPs means that one has no knowledge of the location or clock error states. The n partially known SOPs means that one has knowledge of the location but the clock error states are unknown. The radio SLAM performance bound yields a bound on the uncertainty with which a UAV can localize itself and map the environment while estimating the clock error terms over a finite-time horizon. The following assumptions are necessary to ensure that uniform controllability and observabililty conditions are satisfied simultaneously.

A4. The environment contains a UAV-mounted receiver with imperfect knowledge of its initial states with $n \geq 2$ partially known SOP towers and $m \geq 1$ unknown SOP towers, i.e., the necessary observability condition $l \geq \frac{4+2n+4m}{n+m}$ is satisfied.

A5. The $m \geq 1$ unknown SOP spatial states' process noise terms contain a small non-zero value ($\epsilon \ll 1$) to ensure the covariance is a positive-definite matrix.

A. Studied Scenario

The following motivating scenario is considered. A UAV-mounted receiver is flying in a environment with initial access to GNSS signals from which an imperfect initial state estimate is calculated. GNSS signals became unavailable. Subsequently, the receiver produces pseudorange measurements from ambient terrestrial SOPs. The pseudorange measurements are fused through an EKF to estimate the states of both the (partially known and unknown) SOPs and UAV.

B. Boundedness of EKF Estimation Error Covariance

A uniform lower bound on the state covariance for a LTV stochastic system is valid when both uniform controllability and observability are satisfied simultaneously [**?**, 35]. Put another way, both the controllability and observability Grammians must be full rank (e.g., positive definite). These EKF estimation error covariance bounds have the following form

$$\left(\boldsymbol{\mathcal{O}}_{k,k-l} + \boldsymbol{\mathcal{C}}_{k,k-l}^{-1}\right)^{-1} \preceq \mathbf{P}_k, \tag{7}$$

where

$$\boldsymbol{\mathcal{C}}_{k,k-l} = \sum_{i=k-l}^{k-1} \boldsymbol{\Phi}(k,i+1)\mathbf{Q}\boldsymbol{\Phi}(k,i+1)^{\mathsf{T}} \text{ and } \boldsymbol{\mathcal{O}}_{k,k-l} = \sum_{i=k-l}^{k-1} \boldsymbol{\Phi}(i,k)^{\mathsf{T}}\mathbf{H}(i)^{\mathsf{T}}\bar{\mathbf{R}}^{-1}\mathbf{H}(i)\boldsymbol{\Phi}(i,k) \tag{8}$$

are the controllability and observability Grammians, respectively. To simplify the upcoming derivation, the measurement noise covariance is assumed to be $\bar{\mathbf{R}} \triangleq \sigma^2\mathbf{I}_{M\times M}$, where $\sigma \triangleq \max\{\sigma_{s_1},\ldots,\sigma_{s_m}\}$.

C. Theoretical Lower Bound on the EKF Estimation Error Covariance

The controllability and observability Grammians will be constructed at $l = 4$ epochs to the M terrestrial SOP towers based on the observability analysis in Section III. The Grammians matrices were computed to be

$$\boldsymbol{\mathcal{C}}_{k,k-4} = \sum_{i=k-4}^{k-1} \boldsymbol{\Phi}(k,i+1)\mathbf{Q}\boldsymbol{\Phi}(k,i+1)^{\mathsf{T}} = \sum_{i=1}^{4} \mathbf{F}^{i-1}\mathbf{Q}\left(\mathbf{F}^{i-1}\right)^{\mathsf{T}}$$

$$\boldsymbol{\mathcal{O}}_{k,k-4} = \frac{1}{\sigma^2}\sum_{i=k-4}^{k-1} \boldsymbol{\Phi}(i,k)^{\mathsf{T}}\mathbf{H}(i)^{\mathsf{T}}\mathbf{H}(i)\boldsymbol{\Phi}(i,k) = \frac{1}{\sigma^2}\sum_{i=1}^{4} \left(\mathbf{F}^{-i}\right)^{\mathsf{T}}\mathbf{H}(k-i)^{\mathsf{T}}\mathbf{H}(k-i)\mathbf{F}^{-i}$$

The controllability Grammian is constructed with linear-time invariant (LTI) matrices $\mathbf{Q}$ and $\mathbf{F}$. Thus, the controllability Grammian $\boldsymbol{\mathcal{C}}_{k,k-4}$ is a constant matrix which is a function of the covariance $\mathbf{Q}$. The observability Grammian matrix is constructed with LTI matrix $\mathbf{F}$ and LTV matrix $\mathbf{H}(k)^{\mathsf{T}}\mathbf{H}(k)$. Thus, the observabililty Grammian is a function of the observation Jacobian $\mathbf{H}(k)^{\mathsf{T}}\mathbf{H}(k)$. Therefore, the EKF estimation error bound defined in (7) is dependent on finding a real number $\bar{\alpha} > 0$ such that $\boldsymbol{\mathcal{O}}_{k,k-4} \preceq \bar{\alpha}\mathbf{I}$. The $\bar{\alpha}$ constant can be defined as the trace of the observability Grammian. A tighter upper-bound on the observability Grammian can be established by finding the maximum eigenvalue, but this is a difficult task since the observability Grammian is a LTV matrix. Therefore, the "looser" upper-bound is considered by defining $\bar{\alpha}$ to be the trace, rather than the maximum eigenvalue, of the observability Grammian. The trace is defined as the sum of all eigenvalues, i.e., $\mathrm{Tr}[\boldsymbol{\mathcal{O}}_{k,k-4}] = \sum_{j=1}^{n_x}\lambda_j$ where n_x is the number of estimated states. Alternatively, the trace is defined to be the sum of the elements along the main diagonal of a matrix.

$$\boldsymbol{\mathcal{O}}_{k,k-4} \preceq \underbrace{\mathrm{Tr}(\boldsymbol{\mathcal{O}}_{k,k-4})}_{\bar{\alpha}}\mathbf{I}, \quad \text{where } \mathrm{Tr}(\boldsymbol{\mathcal{O}}_{k,k-4}) = \frac{1}{\sigma^2}\sum_{i=1}^{n_x}\left[\boldsymbol{\mathcal{O}}_{k,k-4}\right]_{i,i} \tag{9}$$

$$(\bar{\alpha}\mathbf{I} + \boldsymbol{\mathcal{C}}_{k,k-4}^{-1}) \succeq (\boldsymbol{\mathcal{O}}_{k,k-4} + \boldsymbol{\mathcal{C}}_{k,k-4}^{-1})$$

$$\Rightarrow (\bar{\alpha}\mathbf{I} + \boldsymbol{\mathcal{C}}_{k,k-4}^{-1})^{-1} \preceq (\boldsymbol{\mathcal{O}}_{k,k-4} + \boldsymbol{\mathcal{C}}_{k,k-4}^{-1})^{-1} \preceq \mathbf{P}_k \tag{10}$$

Furthermore, the observability Grammian's trace, i.e., $\bar{\alpha} = \text{Tr}(\boldsymbol{\mathcal{O}}_{k,k-4})$, is calculated for the radio SLAM base case with $l \geq \frac{4+2n+4m}{n+m} = \frac{4+2(2)+4(1)}{3} = 4$. The considered scenario makes pseudorange measurements at $l = 4$ epochs to the $M = 3$ terrestrial SOP towers in the environment. Defining matrix $B_i = \mathbf{H}(k-i)\mathbf{F}^{-i}$,

$$\text{Tr}(\boldsymbol{\mathcal{O}}_{k,k-4}) = \frac{1}{\sigma^2}\sum_{i=1}^{4}\text{Tr}(B_i^{\mathsf{T}}B_i) = \frac{1}{\sigma^2}\sum_{i=1}^{4}\sum_{j=1}^{n_x}||b_j||_2^2 \tag{11}$$

where $b_j \ \forall j = 1, \ldots, n_x$ are the columns of matrix B_i. The dynamics matrix has a Jordan form. Thus, it can be written as the summation of an identity matrix and an upper triangle hollow matrix which is only a function of the clock sampling time T, i.e, $\mathbf{F} = \mathbf{I} + \mathbf{F}_T$. It can be shown that $\mathbf{F}_T$ is a nilpotent matrix such that $\mathbf{F}_T^i = 0$, for $i \geq 2$. Therefore, the inverse of the dynamic propagation matrix can be calculated as $\mathbf{F}^{-1} = \mathbf{I} - \mathbf{F}_T$. Similarly, it can be shown that $\mathbf{F}^{\pm i} = \mathbf{I} \pm i\mathbf{F}_T$. These dynamics matrix properties are useful in characterizing the trace of the observability Grammian, as discussed in the following

$$\begin{aligned}
B_i &= \mathbf{H}(k-i)\mathbf{F}^{-i} \\
&= \mathbf{H}(k-i) - i\mathbf{H}(k-i)\mathbf{F}_T \\
&= \begin{bmatrix} \boldsymbol{\xi}_1^{\mathsf{T}}(k-i) & -iT\boldsymbol{\xi}_1^{\mathsf{T}}(k-i) & [1, -iT] & \mathbf{0}_{1\times 2} & \mathbf{0}_{1\times 2} & \mathbf{0}_{1\times 2} \\ \boldsymbol{\xi}_2^{\mathsf{T}}(k-i) & -iT\boldsymbol{\xi}_2^{\mathsf{T}}(k-i) & \mathbf{0}_{1\times 2} & [1, -iT] & \mathbf{0}_{1\times 2} & \mathbf{0}_{1\times 2} \\ \boldsymbol{\xi}_3^{\mathsf{T}}(k-i) & -iT\boldsymbol{\xi}_3^{\mathsf{T}}(k-i) & \mathbf{0}_{1\times 2} & \mathbf{0}_{1\times 2} & -\boldsymbol{\xi}_3^{\mathsf{T}}(k-i) & [1, -iT] \end{bmatrix}, \\
\Rightarrow \text{Tr}(B_i^{\mathsf{T}}B_i) &= \sum_{j=1}^{n_x}||b_j||_2^2 = (1+i^2T^2)\sum_{j=1}^{M}(1+||\boldsymbol{\xi}_j||_2^2) + ||\boldsymbol{\xi}_3||_2^2
\end{aligned}$$

The above results can be generalized for M SOP towers where m of them are unknown and n of them are partially known. It should be noted that $||\boldsymbol{\xi}_j||_2 = 1$ for each SOP tower; as it is defined as the normalized distance between the receiver and each SOP tower. This result can be generalized to the following with m unknown SOPs and n partially known SOPs

$$\text{Tr}(B_i^{\mathsf{T}}B_i) = \sum_{j=1}^{n_x}||b_j||_2^2 = (1+i^2T^2)\sum_{j=1}^{M}(1+||\boldsymbol{\xi}_j||_2^2) + \sum_{j=1}^{m}||\boldsymbol{\xi}_j||_2^2 = 2M(1+i^2T^2) + m$$

Finally, the trace of the observability Grammian for the l epochs that have been taken into account can be calculated.

$$\begin{aligned}
\text{Tr}(\boldsymbol{\mathcal{O}}_{k,k-l}) &= \frac{1}{\sigma^2}\sum_{i=1}^{l}\text{Tr}(B_i^{\mathsf{T}}B_i) \\
&= \frac{l}{\sigma^2}\big[(2M+m) + MT^2\frac{(l+1)(2l+1)}{3}\big] \triangleq \bar{\alpha}(n, m, \sigma^2, T, l)
\end{aligned} \tag{12}$$

The constant value $\bar{\alpha}$ calculated in (12) upper-bounds the observability Grammian where $\bar{\alpha}$ is a function of sampling time, partially known and unknown SOP towers, measurement noise, and l-step. Now, the $\bar{\alpha}$ constant is used to construct the linear time-invariant estimation error covariance with minimal uncertainty based on (10).

$$\mathbf{P}_{\text{LB}} = \left(\bar{\alpha}\mathbf{I} + \boldsymbol{C}_{k,k-l}^{-1}\right)^{-1}$$

This uniform lower bound on $\mathbf{P}_k$ is valid with assumptions A1 − A5 to simultaneously guarantee the necessary uniform controllability and uniform observability conditions for estimation error covariance matrix boundedness.

D. Simulation Results

This subsection presents simulation results demonstrating the derived theoretical lower bound for the radio SLAM base case. The UAV is flying at a fixed altitude with velocity random walk dynamics. During the flight, the UAV will draw and fuse pseudorange measurements obtained from $M = 3$ SOP towers detected within a local neighborhood of the UAV. The simulation settings are summarized in Table I.

TABLE I
SIMULATION SETTINGS FOR THE RECEIVER AND EACH SOP FOR RADIO SLAM

Parameter	Value
$\{n, m\}$	$\{2, 1\}$
$\boldsymbol{x}_r(0\|0)$	$[0, 50, 15, -1, 100, 10]^\mathsf{T}$
$\mathbf{P}_r(0\|0)$	$\text{diag}[25, 25, 9, 9, 30 \times 10^3, 3 \times 10^3]$
$\hat{\boldsymbol{x}}_r(0\|0)$	$\sim \mathcal{N}\left[\boldsymbol{x}_r(0\|0), \mathbf{P}_r(0\|0)\right]$
$\boldsymbol{r}_{s_i}(0)$	$\sim [\mathcal{U}[-100, 1000],\ \mathcal{U}[-300, 300]]^\mathsf{T}$
$\{\boldsymbol{x}_{s_i}(0)\}_{i=1}^3$	$\left[\boldsymbol{r}_{s_i}^\mathsf{T}, 1, 0.1\right]^\mathsf{T}$
$\mathbf{P}_s(0\|0)$	$(10^3) \cdot \text{diag}[1, 1, 30, 3]$
$\{\hat{\boldsymbol{x}}_{s_i}(0\|0)\}_{i=1}^3$	$\sim \mathcal{N}\left[\boldsymbol{x}_{s_i}(0), \mathbf{P}_s(0\|0)\right]$
$\{\mathbf{P}_{\text{clk,i}}(0\|0)\}_{i=1}^3$	$(10^3) \cdot \text{diag}[30, 3]$
$\{h_{0,\text{r}},\ h_{-2,\text{r}}\}$	$\left\{9.4 \times 10^{-20},\ 3.8 \times 10^{-21}\right\}$
$\{h_{0,\text{s}_i},\ h_{-2,\text{s}_i}\}_{i=1}^3$	$\left\{8.0 \times 10^{-20},\ 4.0 \times 10^{-23}\right\}$
$\tilde{q}_x, \tilde{q}_y$	$0.1\ \text{m}^2/\text{s}^3$
$\left\{\sigma_{s_i}^2\right\}_{i=1}^3$	$25\ \text{m}^2$
T	$0.1\ \text{s}$

First, results highlighting the uniform estimation performance as a function of unknown SOPs are shown in Fig. 1. To ensure observability, $n = 2$ partially known SOPs are assumed to be known while the m unknown SOPs are varied from 1 to 50 in increments of two. The performance metric used is the A-optimality, which is proportional to the average variance of the estimates [47], given by the trace of the estimation error covariance. It is important to note how the average variance increases as more unknown SOPs are included into the environment. Knowledge of this performance plot can motivate performance-based design or transmitter selection when there is uncertainty about the environment.

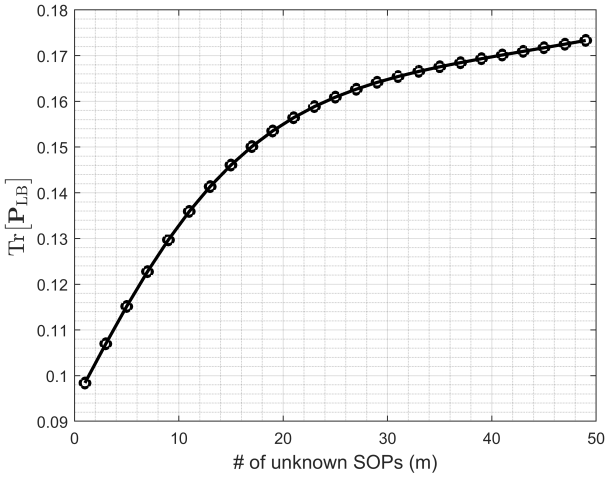

Fig. 1. Uniform estimation performance as a function of unknown SOPs using the A-optimality criteria, i.e., $\text{Tr}[\mathbf{P}_{\text{LB}}]$.

Next, Monte Carlo (MC) simulations with 1000 realizations were conducted to demonstrate the uniform lower bound on the EKF estimation error covariance. The process and measurement noise, initial state estimates, and the SOP

tower locations were randomized for each MC realization. Fig. 2(a) displays the 1σ bounds of $\mathbf{P}(k|k)$ for the UAV and unknown SOP compared to the derived uniform lower bound. Fig. 2(b) displays an eigenvalue point cloud verifying $\mathbf{P}\left(k|k\right) \succeq \mathbf{P}_{\text{LB}}$. It can be seen that, the minimum eigenvalue of the covariance's difference, i.e., $\lambda_{\min}[\mathbf{P}(k|k) - \mathbf{P}_{\text{LB}}]$ will always be greater than or equal to zero at each time step for every MC realization.

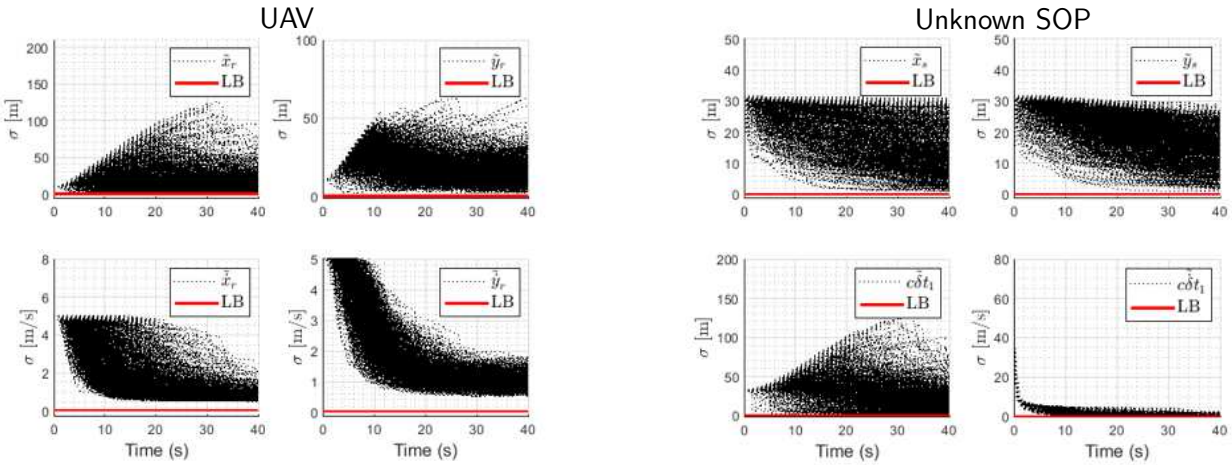

(a) 1σ bounds for localized UAV and unknown SOP

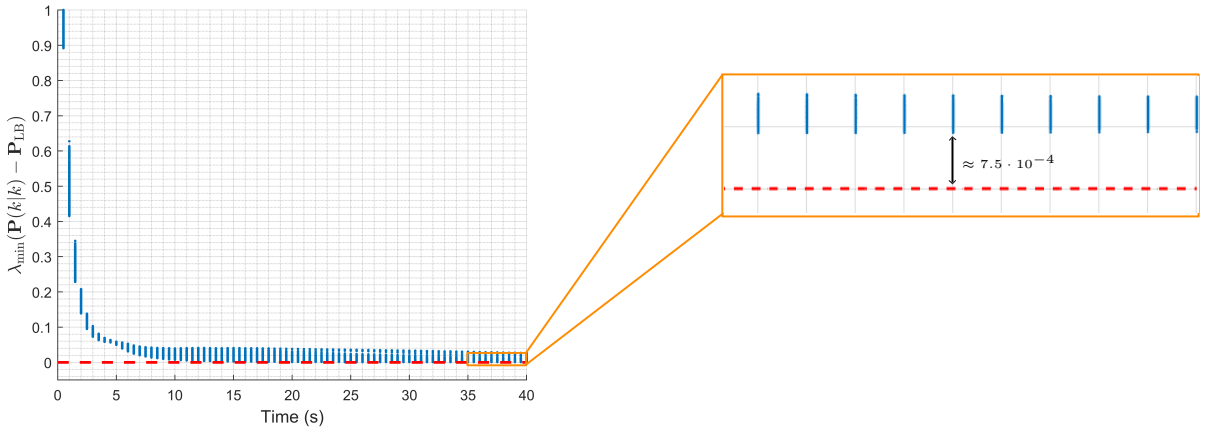

(b) Minimum eigenvalue point-cloud

Fig. 2. MC simulation results for 1000 realizations. (a) 1σ bounds for the EKF estimation error covariance matrix compared with theoretical lower bound. (b) Minimum eigenvalue point cloud verifying $\mathbf{P}\left(k|k\right) \succeq \mathbf{P}_{\text{LB}}$.

V. EXPERIMENTAL RESULTS

A UAV field experiment was conducted in Mission Viejo, CA, USA, to demonstrate the estimation error trajectories and performance for the radio SLAM base case. This section presents the experimental hardware and software setup as well as the radio SLAM results using *only* pseudorange measurements from $M = 3$ SOP towers in the environment.

A. Hardware Setup

The hardware setup for the conducted experiment is shown in Fig. 3. A DJI Matrice 600 drone was equipped with a National Instrument (NI) universal software radio peripheral (USRP)-2955 to sample cellular long-term evolution (LTE) signals at four different carrier frequencies. LTE carrier frequencies 1955, 2145, 2125, and 739 MHz were used for this experiment which are allocated to USA operators AT&T, T-Mobile, and Verizon. The sampling rate was set to 10 MSps and the sampled LTE signals were recorded on a laptop. A Septentrio AsteRx-i V was used to estimate the

position and orientation of the drone which was used as the ground truth. Furthermore, the Spetentrio was equipped with a dual antenna multi-frequency GNSS receiver with RTK and a Vectornav VN-100 micro electromechanical systems (MEMS) inertial measurement unit (IMU).

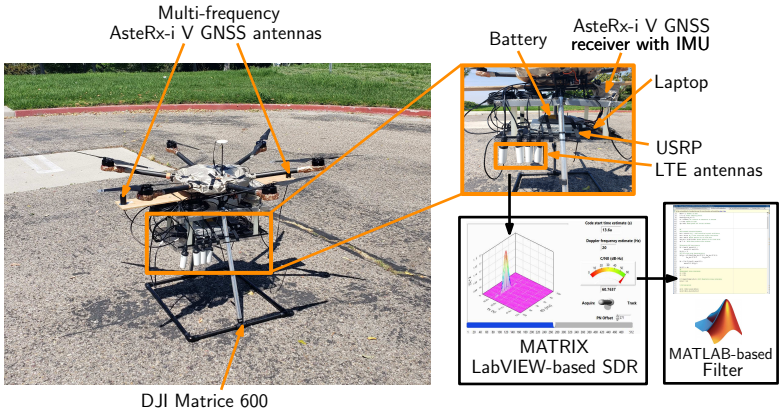

Fig. 3. Experiment hardware setup.

The terrestrial SOP towers' cell IDs and their corresponding carrier frequencies are presented in Table II. The sampled LTE signals were processed offline using the LTE software-defined radio (SDR) proposed in [48]. The resulting measurements were used to simultaneously localize the UAV-mounted receiver and unknown SOP tower while estimating all unknown clock error terms via the radio SLAM framework.

TABLE II
eNodeBs' characteristics

Cell ID	Carrier frequency (MHz)
78	2145
104, 352	1955
308, 358, 224, 58, 354	2125
492, 5, 27	739

B. Software Setup

The UAV's and SOP towers' heights were assumed to be known for the entire duration of the experiment. Therefore, this is a 2-D radio SLAM problem consistent with the observability analysis and performance analysis conducted in Section III and Section IV, respectively. The EKF-based radio SLAM filter was initialized with state estimates and corresponding estimation error covariance given by the following

$$\begin{aligned}
\hat{\boldsymbol{x}}(0|0) &= [0,\ 0,\ 3.42,\ 0.81,\ -539.32,\ 0.16,\ -2237.52,\ 0.55,\ -150.71,\ 91.32,\ -143.11,\ 0.07]\,, \\
\mathbf{P}_r(0|0) &= \mathrm{diag}\left[4,\ 4,\ 1, 1, 30\times 10^6, 3\times 10^3\right], \\
\mathbf{P}_{\mathrm{clk},n}(0|0) &= \mathrm{diag}\left[30\times 10^6,\ 3\times 10^3\right], \quad \mathrm{n}=1,2 \\
\mathbf{P}_{s_3}(0|0) &= \mathrm{diag}\left[7\times 10^4,\ 7\times 10^4, 30\times 10^6,\ 3\times 10^3\right]
\end{aligned}$$

where $\mathbf{P}(0|0)$ was initialized with the initial EKF estimation error covariance matrices listed above. The initial modified clock error terms were solved for by using the initial set of cellular transmitter pseudoranges according to

$$\begin{aligned}
c\delta t_i(0) &= z_{s_i}(0) - \|\boldsymbol{r}_r(0) - \boldsymbol{r}_{s_i}\|_2, \quad i=1,2,3 \\
c\dot{\delta t}_i(0) &= \frac{c\big(\delta t_i(1) - \delta t_i(0)\big)}{T},
\end{aligned}$$

where $\delta t_i(1) = z_{s_i}(1) - \|\boldsymbol{r}_r(1) - \boldsymbol{r}_{s_i}\|_2$ is the modified clock bias at time step $k = 1$. The receiver's clock covariance $\mathbf{Q}_{\text{clk},r}$ was set to correspond to a typical temperature-compensated crystal oscillator (TCXO) with $h_{0,r} = 9.4 \times 10^{-20}$ and $h_{-2,r} = 3.8 \times 10^{-21}$. The i^{th} SOP tower's clock covariance $\mathbf{Q}_{\text{clk},s_i}$ was set to correspond to a typical oven-controlled crystal oscillator (OCXO) with $h_{0,s_i} = 8 \times 10^{-20}$ and $h_{-2,s_i} = 4 \times 10^{-23}$. The UAV's position and velocity states were assumed to evolve according to velocity random walk dynamics where $T = 0.01$ s is the sampling time and $\tilde{q}_x = 1$ m^2/s^3 and $\tilde{q}_y = 20$ m^2/s^3 is the x and y continuous-time acceleration noise spectra whose values were found empirically. The measurement noise was assumed to have a covariance $\mathbf{R} = \sigma^2 \cdot \mathbf{I}_{3\times 3}$, where $\sigma^2 = 30$ m^2 was found empirically.

C. Radio SLAM Results

The UAV traversed a trajectory of 600 m over 175 seconds, while listening to 11 terrestrial SOP towers in the surrounding environment which were mapped prior to conducting the experiment. Although, for the purposes of the radio SLAM case study, only $M = 3$ SOP towers were considered with $n = 2$ partially known SOPs and $m = 1$ unknown SOP. The UAV-mounted receiver's estimate errors were computed with respect to the RTK-IMU trajectory where the resulting estimation error trajectories and corresponding $\pm 1\sigma$ of the UAV's and the unknown SOP tower's states are shown in Fig. 4. Note, only the $\pm 1\sigma$ bounds are shown to highlight the radio SLAM base case estimation performance.

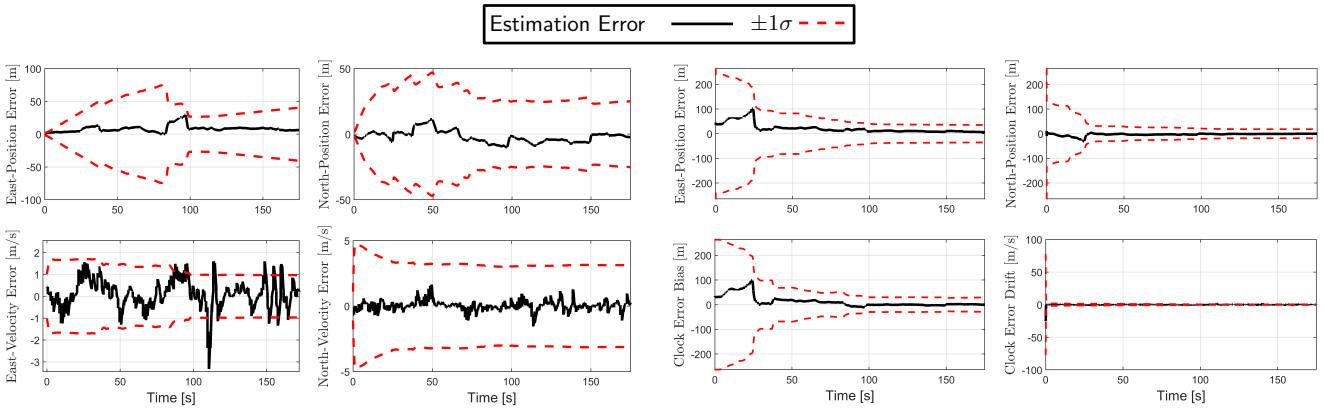

Fig. 4. Radio SLAM base case experimental results showing the estimation error trajectories and corresponding $\pm 1\sigma$ bounds.

The experiment layout contains three cellular SOP tower locations and the true and estimated UAV trajectories as shown in Fig. 5(a). A comparison between the estimated UAV trajectory and the RTK-IMU solution trajectory is shown in Fig. 5(b). The UAV achieved a position root-mean squared error (RMSE) of 10.76 m after traversing the full trajectory. The north-east 95$^{\text{th}}$-percentile initial and final uncertainty ellipses corresponding to SOP tower 3 have a noticeable reduction in size by the end of the experiment. Moreover, the initial 2-D SOP tower position error was 41.57 m, but was eventually reduced to a final 2-D SOP tower position error of 6.62 m, as shown in Fig. 5(c). Furthermore, it should be noted that the radio SLAM error trajectories and performance results were all consistent with the theory and simulation results presented in Section IV.

VI. CONCLUSION

This paper derived a lower bound for the radio SLAM framework. An observability analysis of a UAV with imperfect knowledge of its initial state with two partially known and one unknown SOP towers in the environment (i.e., base case) was assessed and found to be observable for $l \geq 4$ time-steps. Furthermore, a lower bound for radio SLAM's EKF estimation error covariance was derived. Through both single-realization and MC simulations, the lower bound was demonstrated numerically. The experimental results showed a UAV navigating via radio SLAM with signals from two partially known cellular SOPs and one unknown cellular SOP. The achieved results demonstrated bounded localization errors and bounded estimation error variance for 175 seconds without GNSS, in which a trajectory of 600 m was traversed with a position RMSE of 10.76 m.

Fig. 5. (a) Experiment layout containing the true locations of each SOP tower and the two UAV navigation solutions. (b) UAV trajectory comparison between the RTK-IMU navigation solution (red) and radio SLAM (blue). (c) Initial and final position estimates with their associated north-east uncertainty ellipse for SOP tower 3. Map data: Google Earth.

ACKNOWLEDGMENT

This research was supported in part by the Office of Naval Research (ONR) under Grant N00014-19-1-2613 and Grant N00014-19-1-2511, in part by the National Science Foundation (NSF) under Grant 1929965, and in part by Sandia National Laboratories under the Laboratory-Directed Research and Development (LDRD) award.

References

[1] N. Zhu, J. Marais, D. Betaille, and M. Berbineau, "GNSS position integrity in urban environments: A review of literature," *IEEE Transactions on Intelligent Transportation Systems*, vol. 19, no. 9, pp. 2762–2778, September 2018.
[2] A. Broumandan, J. Nielsen, and G. Lachapelle, "Indoor GNSS signal acquisition performance using a synthetic antenna array," *IEEE Transactions on Aerospace and Electronic Systems*, vol. 47, no. 2, pp. 1337–1350, April 2011.
[3] M. Psiaki and T. Humphreys, "GNSS spoofing and detection," *Proceedings of the IEEE*, vol. 104, no. 6, pp. 1258–1270, June 2016.
[4] D. Borio, F. Dovis, H. Kuusniemi, and L. Presti, "Impact and detection of GNSS jammers on consumer grade satellite navigation receivers," *Proceedings of the IEEE*, vol. 104, no. 6, pp. 1233–1245, February 2016.
[5] A. Soloviev, "Tight coupling of GPS, INS, and laser for urban navigation," *IEEE Transactions on Aerospace and Electronic Systems*, vol. 46, no. 4, pp. 1731–1746, October 2010.
[6] M. Moussa, A. Moussa, and N. El-Sheimy, "Multiple ultrasonic aiding system for car navigation in gnss denied environment," in *Proceedings of IEEE/ION Position, Location and Navigation Symposium*, 2018, pp. 133–140.
[7] M. Li and A. Mourikis, "High-precision, consistent EKF-based visual-inertial odometry," *International Journal of Robotics Research*, vol. 32, no. 6, pp. 690–711, May 2013.
[8] M. Shelley, "Monocular visual inertial odometry," Master's thesis, Technical University of Munich, Germany, 2014.
[9] "Position, navigation, and timing technologies in the 21st century," J. Morton, F. van Diggelen, J. Spilker, Jr., and B. Parkinson, Eds. Wiley-IEEE, 2021, vol. 2, Part D: Position, Navigation, and Timing Using Radio Signals-of-Opportunity, ch. 35–43, pp. 1115–1412.
[10] J. McEllroy, "Navigation using signals of opportunity in the AM transmission band," Master's thesis, Air Force Institute of Technology, Wright-Patterson Air Force Base, Ohio, USA, 2006.

[11] M. Psiaki and B. Slosman, "Tracking of digital FM OFDM signals for the determination of navigation observables," in *Proceedings of ION GNSS Conference*, September 2019, pp. 2325–2348.
[12] J. del Peral-Rosado, R. Raulefs, J. López-Salcedo, and G. Seco-Granados, "Survey of cellular mobile radio localization methods: From 1G to 5G," *IEEE Communications Surveys Tutorials*, vol. 20, no. 2, pp. 1124–1148, 2018.
[13] C. Yang and A. Soloviev, "Mobile positioning with signals of opportunity in urban and urban canyon environments," in *IEEE/ION Position, Location, and Navigation Symposium*, April 2020, pp. 1043–1059.
[14] M. Neinavaie, J. Khalife, and Z. Kassas, "Cognitive opportunistic navigation in private networks with 5G signals and beyond," *IEEE Journal of Selected Topics in Signal Processing*, 2021, accepted.
[15] A. Abdallah and Z. Kassas, "UAV navigation with 5G carrier phase measurements," in *Proceedings of ION GNSS Conference*, September 2021, accepted.
[16] P. Thevenon, S. Damien, O. Julien, C. Macabiau, M. Bousquet, L. Ries, and S. Corazza, "Positioning using mobile TV based on the DVB-SH standard," *NAVIGATION, Journal of the Institute of Navigation*, vol. 58, no. 2, pp. 71–90, 2011.
[17] L. Chen, P. T. G. Seco-Granados, O. Julien, and H. Kuusniemi, "Analysis on the TOA tracking with DVB-T signals for positioning," *IEEE Transactions on Broadcasting*, vol. 62, no. 4, pp. 957–961, December 2016.
[18] Z. Kassas, J. Morales, and J. Khalife, "New-age satellite-based navigation – STAN: simultaneous tracking and navigation with LEO satellite signals," *Inside GNSS Magazine*, vol. 14, no. 4, pp. 56–65, 2019.
[19] F. Farhangian, H. Benzerrouk, and R. Landry, "Opportunistic in-flight INS alignment using LEO satellites and a rotatory IMU platform," *Aerospace*, vol. 8, no. 10, pp. 280–281, 2021.
[20] M. Psiaki, "Navigation using carrier doppler shift from a LEO constellation: TRANSIT on steroids," *NAVIGATION, Journal of the Institute of Navigation*, vol. 68, no. 3, pp. 621–641, September 2021.
[21] S. Kozhaya, J. Haidar-Ahmad, A. Abdallah, S. Saab, and Z. Kassas, "Comparison of neural network architectures for simultaneous tracking and navigation with LEO satellites," in *Proceedings of ION GNSS Conference*, September 2021, accepted.
[22] R. Faragher and R. Harle, "Towards an efficient, intelligent, opportunistic smartphone indoor positioning system," *NAVIGATION, Journal of the Institute of Navigation*, vol. 62, no. 1, pp. 55–72, 2015.
[23] T. Kazaz, G. Janssen, J. Romme, and A. Van der Veen, "Delay estimation for ranging and localization using multiband channel state information," *IEEE Transactions on Wireless Communications*, pp. 1–16, September 2021.
[24] H. Durrant-Whyte and T. Bailey, "Simultaneous localization and mapping: part I," *IEEE Robotics & Automation Magazine*, vol. 13, no. 2, pp. 99–110, June 2006.
[25] T. Bailey and H. Durrant-Whyte, "Simultaneous localization and mapping: part II," *IEEE Robotics & Automation Magazine*, vol. 13, no. 3, pp. 108–117, September 2006.
[26] C. Yang and A. Soloviev, "Simultaneous localization and mapping of emitting radio sources-SLAMERS," in *Proceedings of ION GNSS Conference*, September 2015, pp. 2343–2354.
[27] J. Morales and Z. Kassas, "Tightly-coupled inertial navigation system with signals of opportunity aiding," *IEEE Transactions on Aerospace and Electronic Systems*, vol. 57, no. 3, pp. 1930–1948, 2021.
[28] Z. Kassas and T. Humphreys, "Receding horizon trajectory optimization in opportunistic navigation environments," *IEEE Transactions on Aerospace and Electronic Systems*, vol. 51, no. 2, pp. 866–877, April 2015.
[29] J. Morales and Z. Kassas, "Stochastic observability and uncertainty characterization in simultaneous receiver and transmitter localization," *IEEE Transactions on Aerospace and Electronic Systems*, vol. 55, no. 2, pp. 1021–1031, April 2019.
[30] J. Khalife and Z. Kassas, "Opportunistic UAV navigation with carrier phase measurements from asynchronous cellular signals," *IEEE Transactions on Aerospace and Electronic Systems*, vol. 56, no. 4, pp. 3285–3301, August 2020.
[31] E. Leitinger, F. Meyer, F. Hlawatsch, K. Witrisal, F. Tufvesson, and M. Win, "A scalable belief propagation algorithm for radio signal based SLAM," *IEEE Transactions on Wireless Communications*, vol. 18, no. 12, pp. 5613–5629, September 2019.
[32] Y. Yang, J. M. J. Khalife and, and Z. Kassas, "UAV waypoint opportunistic navigation in GNSS-denied environments," *IEEE Transactions on Aerospace and Electronic Systems*, p. accepted, 2021.
[33] J. Morales and Z. Kassas, "Event-based communication strategy for collaborative navigation with signals of opportunity," in *Proceedings of Asilomar Conference on Signals, Systems and Computers*, November 2018, pp. 548–553.
[34] J. Morales, J. Khalife, and Z. Kassas, "Information fusion strategies for collaborative inertial radio SLAM," *IEEE Transactions on Intelligent Transportation Systems*, 2021, accepted.
[35] J. Deyst and C. Price, "Conditions for asymptotic stability of the discrete minimum-variance linear estimator," *IEEE Transactions on Automatic Control*, vol. 13, no. 6, pp. 702–705, December 1968.
[36] G. Dissanayake, P. Newman, S. Clark, H. Durrant-Whyte, and M. Csorba, "A solution to the simultaneous localization and map building (SLAM) problem," *IEEE Transactions on Robotics and Automation*, vol. 17, no. 3, pp. 229–241, June 2001.
[37] J. Fenwick, P. Newman, and J. Leonard, "Cooperative concurrent mapping and localization," in *Proceedings of IEEE International Conference on Robotics and Automation*, May 2002, pp. 1810–1817.
[38] Z. Jiang, S. Zhang, and L. Xie, "Cramer-Rao lower bound analysis for mobile robot navigation," in *Proceedings of International Conference on Intelligent Sensors, Sensor Networks and Information Processing*, 2005, pp. 229–234.
[39] A. Mourikis. and S. Roumeliotis, "Analysis of positioning uncertainty in simultaneous localization and mapping (SLAM)," in *Proceedings of IEEE/RSJ International Conference on Intelligent Robots and Systems*, vol. 1, 2004, pp. 13–20.
[40] S. Huang and G. Dissanayake, "Convergence and consistency analysis for extended Kalman filter based SLAM," *IEEE Transactions on Robotics*, vol. 23, no. 5, pp. 1036–1049, October 2007.
[41] T. Karvonen, S. Bonnabel, E. Moulines, and S. Särkkä, "Bounds on the covariance matrix of a class of Kalman-Bucy filters for systems with non-linear dynamics," in *Proceedings of IEEE Conference on Decision and Control*, 2018, pp. 7176–718.
[42] X. Li and V. Jilkov, "Survey of maneuvering target tracking. Part I: Dynamic models," *IEEE Transactions on Aerospace and Electronic Systems*, vol. 39, no. 4, pp. 1333–1364, 2003.
[43] A. Thompson, J. Moran, and G. Swenson, *Interferometry and Synthesis in Radio Astronomy*, 2nd ed. John Wiley & Sons, 2001.
[44] W. Rugh, *Linear System Theory*, 2nd ed. Upper Saddle River, NJ: Prentice Hall, 1996.
[45] R. Hermann and A. Krener, "Nonlinear controllability and observability," *IEEE Transactions on Automatic Control*, vol. 22, no. 5, pp. 728–740, October 1977.
[46] K. Reif, S. Gunther, E. Yaz, and R. Unbehauen, "Stochastic stability of the discrete-time extended Kalman filter," *IEEE Transactions on Automatic Control*, vol. 44, no. 4, pp. 714–728, April 1999.
[47] D. Uciński, *Optimal Measurement Methods for Distributed Parameter System Identification*. CRC Press, 2005.
[48] K. Shamaei and Z. Kassas, "LTE receiver design and multipath analysis for navigation in urban environments," *NAVIGATION, Journal of the Institute of Navigation*, vol. 65, no. 4, pp. 655–675, December 2018.